The effect of sidewall forest canopies on the formation of cold-air pools: A numerical study

M. T. Kiefer[1] and S. Zhong[1]

Received 14 December 2012; revised 18 April 2013; accepted 19 May 2013; published 17 June 2013.

[1] While the evolution and dynamics of cold-air pools in basins and valleys continue to be an active area of research, the influence of vegetation cover on cold-air pools remains largely unexamined. Recently, the Advanced Regional Prediction System (ARPS) atmospheric model has been modified to allow simulation of flow through a multilayer canopy (ARPS-CANOPY). In this study, two-dimensional numerical simulations are performed with ARPS-CANOPY to examine the impact of sidewall forest cover on diurnal cold-air pool formation inside an idealized valley. A cold-air pool develops regardless of the presence or absence of sidewall vegetation. However, the strength of the temperature inversion and the overall cooling appear to be substantially modified by sidewall vegetation. The coldest overall valley temperature occurs with no sidewall vegetation cover while the warmest occurs when the valley sidewalls are fully covered with vegetation. In simulations with partial forest cover, the nocturnal cooling in approximately the upper two thirds (lower one third) of the valley atmosphere is shown to be most sensitive to forest cover along the upper half (lower half) of the sidewall. The sidewall forest cover also affects downslope flows through a combination of weaker surface cooling beneath the forest canopy and increased drag on air flowing down the sidewalls. Finally, the strength of downslope flow is shown to be highly sensitive to the presence or absence of trees farther up the slope.

Citation: Kiefer, M. T., and S. Zhong (2013), The effect of sidewall forest canopies on the formation of cold-air pools: A numerical study, *J. Geophys. Res. Atmos.*, *118*, 5965–5978, doi:10.1002/jgrd.50509.

1. Introduction

[2] A common feature of nocturnal boundary layers in valleys and basins are cold-air pools, defined as topographically confined, stagnant layers of air that are colder than the overlying air [*Whiteman et al.*, 2001]. Cold-air pools may be categorized as diurnal [e.g., *Whiteman et al.*, 1996; *Clements et al.*, 2003] or persistent [e.g., *Whiteman et al.*, 2001; *Steinacker et al.*, 2007], based on the duration of the event. Diurnal cold-air pool formation in valleys and basins has been attributed [*Geiger*, 1965] to radiation loss along sloping terrain that drives a downslope flow of cold air into the developing cold-air pool, amplifying the cooling occurring due to radiative heat loss at the valley or basin floor. While cold-air pools have been shown to form in valleys and basins in the absence of drainage flow [*Thompson*, 1986; *Gustavsson et al.*, 1998], numerous studies have identified slope flows and the resultant accumulation of cold air at the bottom of basins and valleys as a critical source of cold-air pools [e.g., *Barr and Orgill*, 1989; *Mahrt et al.*, 2001; *LeMone et al.*, 2003; *Whiteman et al.*, 2010; *Kiefer and Zhong*, 2011].

[3] Although the development and evolution of cold-air pools in basins and valleys is an active area of research (see, for example, the recent METCRAX field experiment inside Arizona's Meteor Crater [*Whiteman et al.*, 2008]), the influence of vegetation cover on cold-air pools has received little attention. *Gustavsson et al.* [1998] examined the impact of tree cover on observed surface temperatures inside shallow valleys [O(10 m) depth] in southwestern Sweden and found that valleys with forest cover were colder throughout the night than valleys with bare ground. Although evidence of cold-air drainage flows was found in the nonforested valleys, the especially cold temperatures observed inside the forested valleys were attributed to a sheltering effect that reduced turbulent mixing of heat down to the surface. *Gross* [1987] conducted simulations of temperature and wind in a valley in Germany using a mesoscale model (with a canopy submodel) and found simulated temperatures to be colder in the valley with forest cover than in simulations where the tree cover was replaced with grass. Such a finding is rendered dubious by the knowledge that unrealistically strong cooling rates were simulated in the upper canopy, the result of several incorrect assumptions regarding canopy thermodynamic properties (no canopy heat storage term, air and canopy

[1]Department of Geography, Michigan State University, East Lansing, Michigan, USA.

Corresponding author: M. T. Kiefer, Department of Geography, Michigan State University, 1407 S. Harrison Rd., Rm. 220, East Lansing, MI 48823, USA. (mtkiefer@msu.edu)

2169-897X/13/10.1002/jgrd.50509

heating/cooling rates assumed identical; for more details, see *Froelich et al.* [2011]). The complicated topography in the valley as well as the use of coarse [300 m] grid spacing with steep terrain slopes [as steep as 53%] sheds further doubt on their results.

[4] Although the impact of forest cover on cold-air pool dynamics has received only modest attention, the effect of trees on slope flows has been subject to greater scrutiny by the research community and is thus somewhat better understood. Much of the focus regarding slope flows and forest cover has been with regard to ecosystem-atmosphere exchanges of carbon dioxide and other scalars [e.g., *Goulden et al.*, 1996; *Lee*, 1998; *Aubinet et al.*, 2003; *Froelich et al*., 2005; *Froelich and Schmid*, 2006; *Sun et al.*, 2006; *Belcher et al.*, 2012]. For example, *Froelich and Schmid* [2006] analyzed flux tower data at a densely forested hilly site in Indiana for evidence of nocturnal slope flows inside and above the forest canopy that have been implicated in vertical exchange processes in earlier studies. They showed evidence of downslope flows above the canopy and upslope flows below the tree tops and related such flows to pronounced differences in lapse rates between the two layers. Using a model broadly similar to that of *Gross* [1987], but capable of simulating generally realistic cooling rates inside the canopy, *Sun et al.* [2006] simulated daytime and nighttime slope flows at a forested coastal mountain site in British Columbia with a goal of improving understanding of carbon dioxide transport in complex terrain. Simulated anabatic and katabatic flows were shown to be weaker over forested slopes than over bare slopes and separate sub-canopy and above-canopy flows were noted. The flow separation was attributed in part to strong canopy top cooling and resultant stable stratification above the canopy that prevented mixing of momentum and heat between the canopy atmosphere and overlying air.

[5] Two aspects of slope flows in and above forest canopies emerge from the review of literature. First, flows along forested slopes are generally weaker and displaced upward from the surface, compared to bare or grassy surfaces. Second, the direction of airflow below canopy top may be opposite that of flow above the canopy, given a sufficiently dense forest. Furthermore, two aspects of valley and slope temperatures emerge. First, the limited number of studies examining the role of forest cover in valley cooling have found colder temperatures inside forested valleys. Second, strong canopy top cooling and resultant stable stratification above the canopy can inhibit mixing of above and below canopy katabatic flows and contribute to flow separation.

[6] In this study, we examine the role of sidewall forest cover in modifying cold-air pool evolution and the underlying dynamics. Numerical simulations will be performed for an idealized valley with a scale comparable to large [O(25–50 km) in scale], populated valleys such as the Salt Lake or Tooele valleys in Utah. In contrast to the studies outlined earlier, we will not examine how forest cover affects the exchange of atmospheric constituents, or address the sheltering effect of trees in shallow valleys or basins, although we acknowledge the importance of such research. Given that cold-air pools are known to contribute to air pollution and/or impaired visibility episodes [*Reddy et al.*, 1995; *Smith et al.*, 1997], an improved understanding of how forest cover impacts cold-air pool processes may be beneficial to those managing public and private lands in and around populated valleys known to experience episodes of poor air quality. To achieve the stated goal, we utilize a recently developed canopy flow modeling system, ARPS-CANOPY, which is based on the Advanced Regional Prediction System (ARPS) [*Kiefer et al.*, 2013; *Xue et al.*, 2000, 2001]. Two-dimensional simulations of an idealized valley are performed with forest cover along the valley sidewalls varying from bare to partially forested to completely forested.

[7] The remainder of this paper is organized as follows. Section 2 gives a brief description of ARPS-CANOPY (section 2.1), the model configuration and parameterization used in this study (section 2.2), and the numerical design (section 2.3). Results and discussion of the experiments are presented in section 3, including a general assessment of cold-air pool evolution (section 3.1), an analysis of slope cooling processes (section 3.2), and an assessment of valley cooling processes (section 3.3). Finally, the paper is concluded in section 4.

2. Model Description and Experiment Design

2.1. ARPS-CANOPY Summary

[8] ARPS is a three-dimensional, compressible, nonhydrostatic atmospheric model with a terrain-following coordinate system. ARPS is well suited to multiscale simulations, with the model having been applied with grid spacing as fine as O(1 m) by *Dupont and Brunet* [2008, 2009], while having also been applied with much coarser grid spacing to mesoscale to synoptic scale phenomena [e.g., *Xue et al*., 2003; *Parker and Johnson*, 2004; *Michioka and Chow*, 2008]. ARPS has been shown in a number of studies to be capable of simulating the salient features of observed downslope flows, including katabatic flows over gentle bare slopes [e.g., *Chen et al.*, 2004; *Smith and Skyllingstad*, 2005; *Trachte et al.*, 2010; *Kiefer and Zhong*, 2011]. However, the standard ARPS formulation lacks the capability to simulate atmospheric variables within a multilayer canopy. In the ARPS framework, as with many mesoscale models, the bulk effect of a vegetation canopy on the free atmosphere is computed within a single layer, beneath the lowest model grid point.

[9] A modified version of ARPS was developed by *Kiefer et al.* [2013], based on earlier modifications to ARPS made by *Dupont and Brunet* [2008], to account for the effects of vegetation elements on flow through a multilayer canopy. Following *Dupont and Brunet* [2008], a term was added to the momentum equation to account for drag that occurs due to the presence of the canopy elements, and a term was added to the subgrid-scale (SGS) turbulent kinetic energy (TKE) equation to account for the enhancement of turbulence dissipation in the canopy air space. Following *Kanda and Hino* [1994], a production term was also added to the SGS TKE equation to represent the production of SGS TKE in the wakes of canopy elements, at scales large enough that the turbulence does not dissipate immediately yet small enough that it remains unresolved. Regarding the impact of the canopy elements on heating/cooling processes inside the canopy layer and shading of the ground surface, changes to the ARPS radiation parameterization were made following work by *Sun et al.* [2006]. First, a set of equations were added to the radiation physics module to compute net

radiation flux at canopy top and then a profile of net radiation was prescribed that assumes an approximately exponential decay within the canopy. Second, a term was added to the thermodynamic equation to represent heating (cooling) of the canopy air spaces that results from the vertical flux convergence (divergence) of net radiation absorbed by the canopy elements. Lastly, the ground net radiation flux was reduced, by a factor proportional to the density of the canopy, to account for shading by the overlying vegetation during the day and reduction of outgoing longwave ground radiation at night.

[10] We wish to emphasize here that ARPS-CANOPY does not resolve the flow around individual trees or the heating/cooling of individual branches or leaves. From canopy drag and turbulence production to canopy shading and heating/cooling of the canopy air space, the canopy is represented in the model as a height-varying plant area density profile (A_p), specified at each grid point. A_p, defined as the one-sided area of all plant material per unit volume of canopy, is a bulk measure of the density of a large group of trees. Note in this study we apply the same A_p profile at every grid point categorized as forested. However, it is possible with ARPS-CANOPY to specify a different A_p profile at each grid point, and the model is even capable of ingesting three-dimensional arrays of A_p from an external file.

2.2. Model Configuration and Parameterization

[11] Outside of the modifications outlined in the prior section, ARPS-CANOPY is otherwise identical to standard ARPS. A 1.5-order subgrid-scale turbulence closure scheme with a prognostic equation for the turbulent kinetic energy is utilized, as well as radiation physics following *Chou* [1990, 1992] and *Chou and Suarez* [1994], however, with computation of the canopy source term and attenuation of net radiation inside the canopy applied as discussed in section 2.1. Fourth-order accurate finite differencing of the advection terms is used in both the vertical and horizontal directions, while the upper boundary condition for all simulations is a sponge layer extending from z = 6.1 km to the model top at z = 8 km. Due to the regional-scale domain size, the Coriolis force is computed (as a function of central latitude only). However, moist processes are omitted in all simulations.

[12] A two-dimensional computational domain has been utilized in this study to enable the use of the fine resolution required to resolve small-scale canopy flows and turbulent motions in the nocturnal valley atmosphere, but simultaneously keep the simulations computationally feasible. Use of a two-dimensional framework also allows us to focus on slope flows without the complication of along-valley flows or any other three-dimensional topographic flows, rendering the outcome of the sensitivity experiments potentially less ambiguous. The model domain extends 110 km in the x direction and 8 km in the z direction, with horizontal grid spacing of 30 m and vertical grid spacing of 2 m up to a height of 54 m, above which vertical stretching is applied.

[13] For all simulations, ARPS has a horizontally homogeneous initial condition. A base state sounding consisting of quiescent wind and neutral static stability (below the sponge layer; stable stratification above 6.1 km) is utilized for all experiments. The latitude/longitude of the domain center, time of local sunset, and soil characteristics are representative of western Colorado during mid-August, although the location and time of year are chosen arbitrarily and the results are not meant to be location specific. The model is initialized approximately 1 h following local sunset and is run for a total of 9 h to simulate the development of the nocturnal cold-air pool. Note that we avoid simulation of the evening transition period due to concerns about applying ARPS-CANOPY to a time of day when the rates of change of air temperature and canopy element temperature are expected to be highly dissimilar [*Froelich et al.*, 2011]. ARPS-CANOPY overestimates cooling in the air spaces between vegetation elements during time periods when canopy element cooling rates are large, such as during the evening transition period; this is a known limitation of ARPS-CANOPY [*Kiefer et al.*, 2013] as well as other models with similar canopy heat source parameterizations [e.g., *Sun et al*., 2006].

2.3. Experiment Design

[14] Four experiments are conducted in this study in which forest cover over valley sidewalls is varied between completely bare and completely forested (Figure 1). In experiments NC (No Canopy) and FC (Full Canopy), the valley sidewalls are bare and fully forested, respectively, while in experiments LC (Lower Canopy) and UC (Upper Canopy), forest cover is restricted to the lower and upper halves of the sidewalls, respectively. The LC and UC cases represent valleys where trees are unable to grow above or below a particular elevation because the local climate there is inhospitable to tree growth (e.g., too dry, too cold or hot). Although valleys with bare sidewalls above a tree line (i.e., LC case) are common features of high terrain (e.g., Rockies, Alps), valleys with bare sidewalls at lower elevations (i.e., UC case) are not uncommon (e.g., the region where the Sierra Nevada mountains border the lower elevations of western Nevada, the terrain around Flagstaff, Arizona). At each point designated as forested, the plant area density profile is specified as in Figure 1e, with a plant area index (PAI; vertically integrated plant area density) equal to 2, and a canopy height of 18 m. This profile is identical to the case 1 profile used by *Dupont and Brunet* [2008] and is representative of trees of moderate density, but is not intended to represent any particular species of tree. The tree fraction in each grid cell, a model parameter specified in ARPS-CANOPY, is set to 75% in all experiments (i.e., gaps between trees are assumed to constitute 25% of each forested grid cell). Thus, wherever the terms "full" and "partial" are used in this paper to describe the forest canopy cover along the sidewall, the terms refer not to fraction of each grid cell covered in trees, but to the proportion of the sidewall slope covered with forest. However, within each grid cell categorized as forested, the canopy is assumed to be horizontally homogeneous.

[15] For all experiments, the topography consists of a central valley surrounded on either side by bell-shaped mountains of height 500 m and half width 10 km. The width of the valley, as measured from peak to peak, is 30 km, and the sidewall slope is 5%. Such a slope is well suited to the generation of slope flows in our simulations;

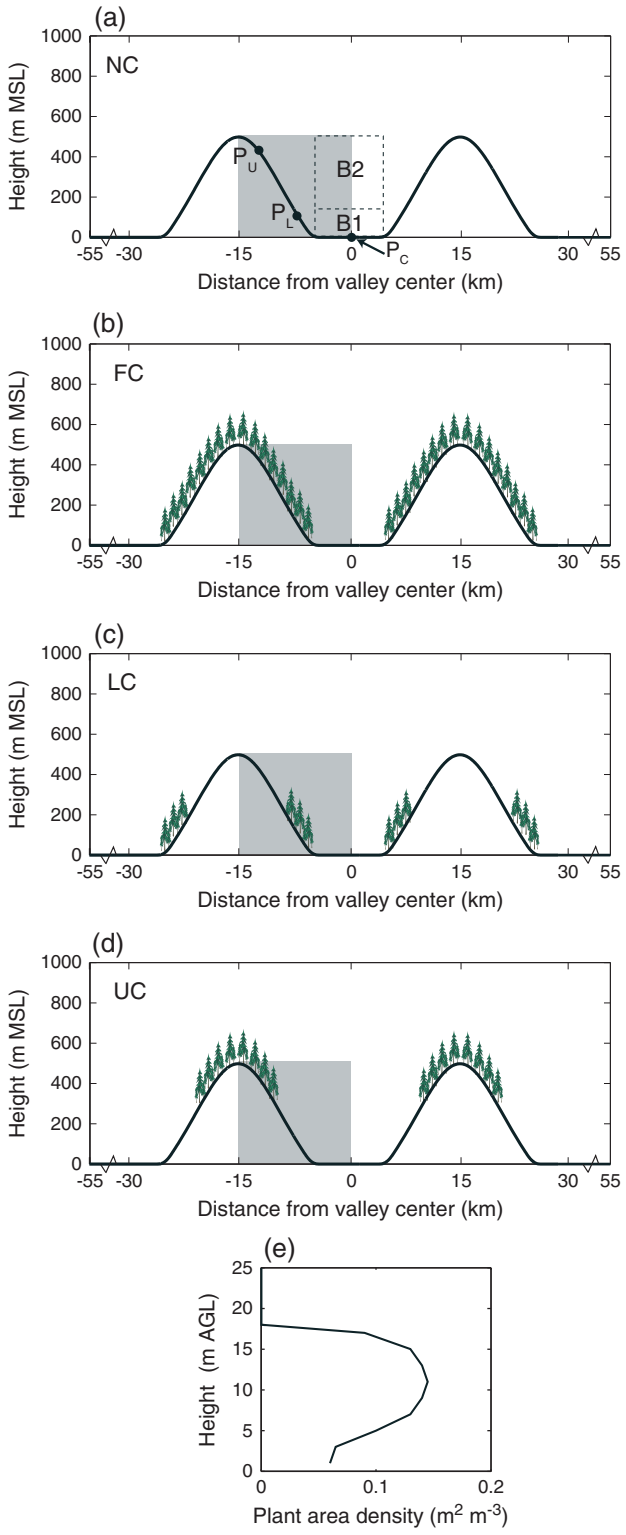

Figure 1. Summary of (a–d) experiments and (e) plant area density profile. In Figure 1a, points used for vertical profile and time series analysis in section 3.2 are indicated with filled circles, and valley sub-zones used for bulk cooling analysis in section 3.3 are denoted by labeled squares. The shaded gray box denotes the area of the domain shown in Figure 2. Note that the canopy layer is exaggerated vertically for clarity.

shallower slopes would require a longer distance (and possibly a larger domain) for flows to develop and steeper slopes are likely to inhibit a well-developed katabatic flow [*Zhong and Whiteman*, 2008]. Recall that the model domain is two dimensional with periodic lateral boundary conditions in the *y* direction (i.e., along the valley axis). Thus, the valley is assumed to be infinitely long and cold-air drainage out of the valley is not simulated. Cooling rates simulated in this study may be exaggerated compared to valleys where cold air can drain out of the valley system.

3. Results and Discussion

3.1. Cold-Air Pool Overview

[16] We begin by examining vertical cross sections of potential temperature and the *u* component of the wind from each of the four cases, at time T06 (where "06" refers to the hour after initialization) (Figure 2). In this and all subsequent analyses, we focus on the west half of the valley due to symmetry around the valley center, a result of the idealized model configuration. At this mature stage of the cold-air pool evolution, broad differences between cases are evident. Assessing the potential temperature first (Figure 2, left), we see that the cold-air pool is strongest (i.e., coldest and deepest) in the NC case and weakest (i.e., warmest and shallowest) in the FC case. Regarding the intermediate forest cover cases, LC and UC, the cold-air pool is stronger in the UC case, although potential temperatures in the upper two thirds of the valley are actually colder in the LC case.

[17] Regarding the *u* component of the wind (Figure 2, right), we find a stronger downslope jet (∼4–5 m s^{-1}) in the NC and LC cases and a weaker jet (∼3–4 m s^{-1}) in the FC and UC cases, although it is difficult to assess which specific case has the strongest or weakest jet from the vertical cross sections alone. What is apparent is that the jet is displaced from the surface wherever trees exist along the slope; this phenomenon results in a sudden jump in jet height at the mid-slope point in the LC case, with a corresponding compression in jet height seen in the UC case. Note that the downslope winds simulated in this study are well within the range of what has been observed over gently sloping terrain during recent field campaigns (e.g., VTMX, *Whiteman and Zhong* [2008] and METCRAX, *Savage et al.* [2008]). Furthermore, the findings regarding the weaker magnitude and upward displacement of the jet, relative to downslope flows over bare ground, are consistent with observational and numerical modeling studies [e.g., *Gross*, 1987; *Froelich and Schmid*, 2006; *Sun et al.*, 2006; *Belcher et al.*, 2012]. Note that away from the sidewalls, winds are weak (±0.75 m s^{-1}). In the upper valley, this is the result of the quiescent initialization of ARPS; the weak nature of winds within the bottom of the valley is a consistent feature of cold-air pools [e.g., *Whiteman et al.*, 2001, 2008; *Clements et al.*, 2003].

[18] In the four experiments examined in this study, forest cover is restricted to the valley sidewalls. Although the focus of this study is on sidewall forest cover, it is worth commenting on the impact of valley-floor forest cover on the cold-air pool process. In an additional experiment with forest cover on the sidewalls and valley floor, potential temperatures were 2–3 K warmer near the valley floor, relative to

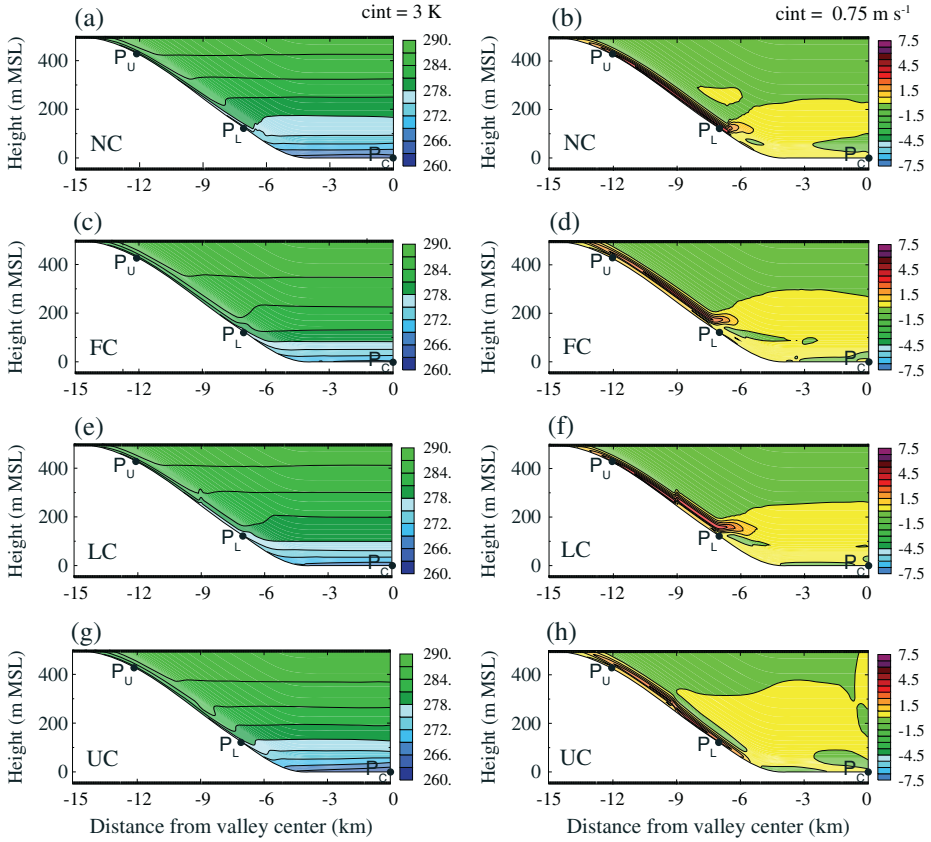

Figure 2. Vertical cross sections of (a, c, e, g) potential temperature (K) and (b, d, f, h) *u* wind component (m s^{-1}) inside the west half of the valley, at T06. The location of points used for vertical profile and time series analyses are denoted by small circles: P_U, P_L, and P_C.

the FC case, whereas downslope flow and valley cooling away from the floor were minimally impacted (not shown). Warmer potential temperatures are associated with reduced sky view factor and thus weaker radiative cooling of the valley floor (relative to no forest cover). Since the downslope flow and bulk cooling of the valley are largely unaffected by forest cover at the valley floor, we proceed with the four sidewall cover experiments, but caution that the results of this additional experiment should be taken into account when interpreting results from the sidewall forest cover experiments.

[19] In order to examine the vertical structure of the cold-air pool and its evolution during the simulation in greater detail, we now consider vertical profiles at three points, one along the upper slope (P_U), a second along the lower slope (P_L), and a third at the valley center (P_C). Beginning with potential temperature (Figure 3), it is apparent that cooling at all three points is mainly restricted to the valley atmosphere [at or below 500 m above mean sea level (MSL)], and at P_U, within 50 m of the sloped surface. Comparing the four cases, we see that throughout the simulation, the coldest potential temperatures occur in the NC case, and the warmest temperatures occur in the FC case. Upon examining the intermediate case profiles at P_C (Figures 3c, 3f, and 3i), an interesting phenomenon becomes apparent. Below approximately 180 m msl, the potential temperature is consistently colder in case UC than LC, while above that height, the opposite behavior is noted. A similar "crossover" point is also apparent at P_L during the last 6 h of the simulation (Figures 3e and 3h), at a level near or slightly higher than 200 m msl. Closer to the sloped surface at P_L, the difference in potential temperature between cases is smaller and the relationship between cooling and forest cover is less clear. Analysis of the thermodynamic budget within the canopy layer is discussed in section 3.2. The underlying thermodynamic forcing behind the crossover point will be examined in detail in section 3.3.

[20] Cooling of the sloped surface promotes the development of a downslope flow, which is depicted at the three analysis points in Figure 4. Considering point P_U first, a clear relationship between forest cover and slope wind speed is evident: Cases with bare upper slopes (NC, LC) exhibit winds 1–1.5 m s^{-1} stronger than cases with forested upper slopes (FC, UC). Furthermore, the jet is displaced upward away from the surface in cases with forest cover on the upper slope, with a small secondary maximum in wind speed at the surface (below the thickest part of the forest canopy). Winds are weakest in the middle of the canopy where the parameterized drag by canopy elements is strongest. Note that although these results are broadly consistent with earlier research studies [*Belcher et al.*, 2012], there is no evidence of upslope flow near the bottom of the canopy [e.g., *Froelich and Schmid*, 2006]. The lack of upslope near-surface flow is consistent with the use of a relatively thin canopy and

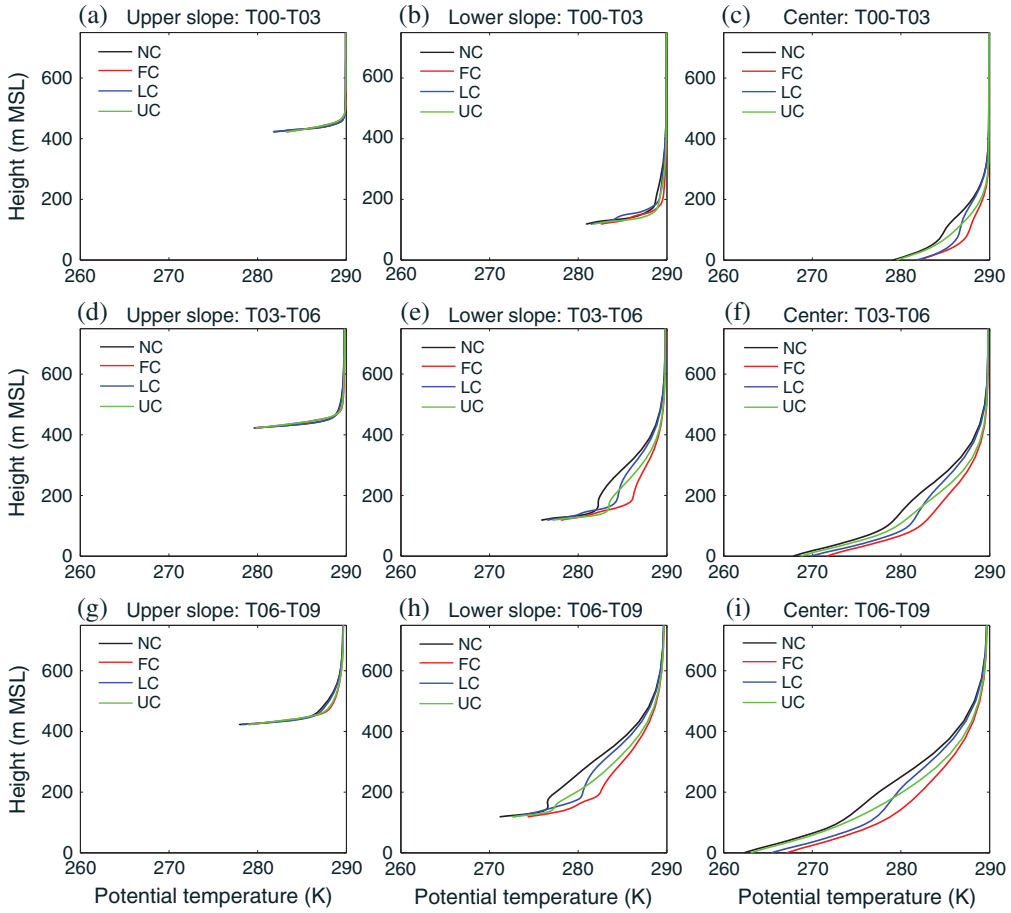

Figure 3. Three hour average potential temperature profiles at points (a, d, g) P_U, (b, e, h) P_L, and (c, f, i) P_C. (top) Fields averaged from T00 to T03, (middle) T03–T06, and (bottom) T06–T09.

the lack of any unstably stratified layer beneath the forest canopy. Further down the slope, at point P_L, the comparison is a bit more complicated. While the NC and FC cases exhibit the strongest and weakest jets, respectively, we find a stronger downslope jet along the upper slope in the LC case, compared to the UC case, and as a result, the downslope flow along the lower slope is stronger in the LC case than the UC case. Although the comparison is at a single point, an examination of the jets in the LC and UC cases in Figure 2 (cf. Figures 2f and 2h) confirms the relative weakness of the UC jet. Thus, from this analysis alone, it appears that the state of forest cover on the upper slopes has a pronounced impact on slope flow on both the upper and the lower half of the mountain.

3.2. Slope Cooling Analysis

[21] With the cold-air pool general assessment completed, we now focus our attention on the cooling of the atmosphere immediately above the sloped surface and the evolution of the aforementioned downslope flow. Figure 5 depicts the nocturnal evolution of potential temperature averaged over the lowest 18 m of the atmosphere (corresponding to the canopy layer in the cases where trees are present) and the maximum u component of wind speed, at points P_L and P_U. Along the upper slope (Figures 5a and 5b), we see that as with the vertical profiles, the time series interpretation is relatively straightforward: Cooling during the first 1.5 h of the simulation is stronger in the cases with bare upper slopes (NC and LC cases) and the downslope flow is consistently stronger in those cases. Along the lower slope (Figures 5c and 5d), cooling during approximately the first 45 min is stronger in the cases with bare lower slopes (NC and UC cases), but cooling in the LC case (forested lower slopes) quickly catches up (see inset panel in Figure 5c). Furthermore, while the development of the downslope jet occurs more quickly in the cases with bare lower slopes (NC and UC), the jet in the LC case becomes stronger than the jet in the UC case after about 45 min of simulation time. Such findings point to the important role of the upper slope forest cover on the flow along the lower slopes. When the upper slopes are bare and the lower slopes are forested, the cooling of the upper slope drives a well-developed downslope flow that impinges on the forested lower slope; in the opposite scenario, a relatively weak jet develops above the forested upper slopes and impinges on the bare lower slope, but is unable to reach the same strength as the jet that forms when the upper slopes are bare.

[22] An examination of the thermodynamic budget near the mountain slope can provide much needed insight into the cooling of the air along the slopes (and indirectly, the

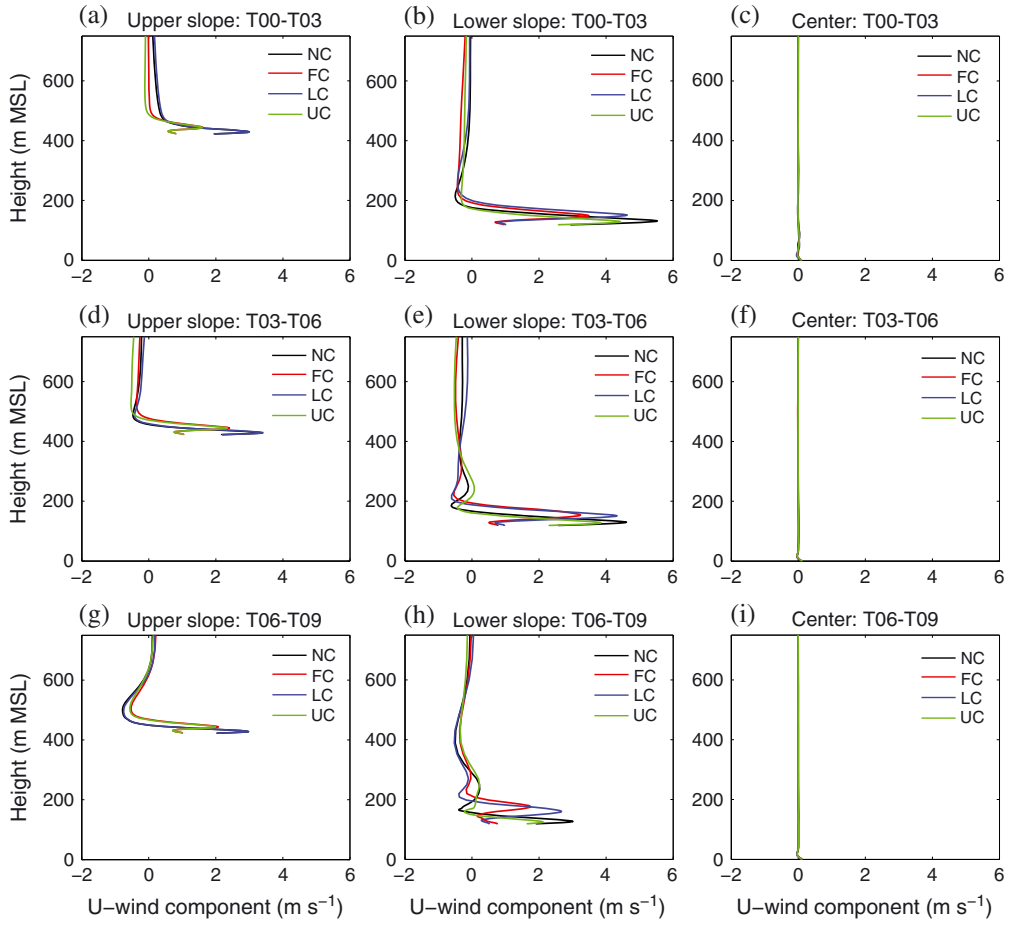

Figure 4. As in Figure 3 but for the *u* component of wind.

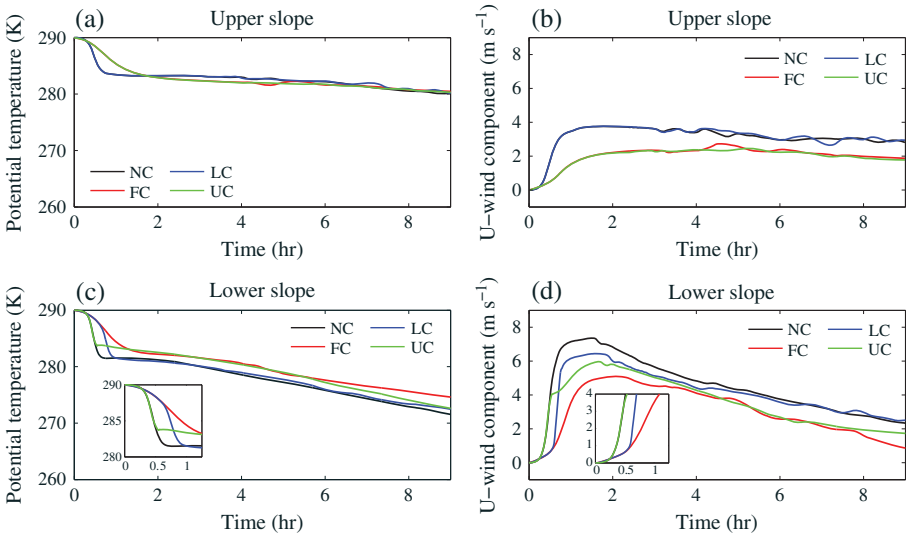

Figure 5. Time series of (a, c) potential temperature averaged from the surface to 18 m agl and (b, d) maximum *u* component of wind speed, at points P_U and P_L. The maximum speed is the maximum wind speed in the downslope flow at a particular point. Inset panels in Figures 5c and 5d are included to enhance clarity of features during the first 75 min of the simulation.

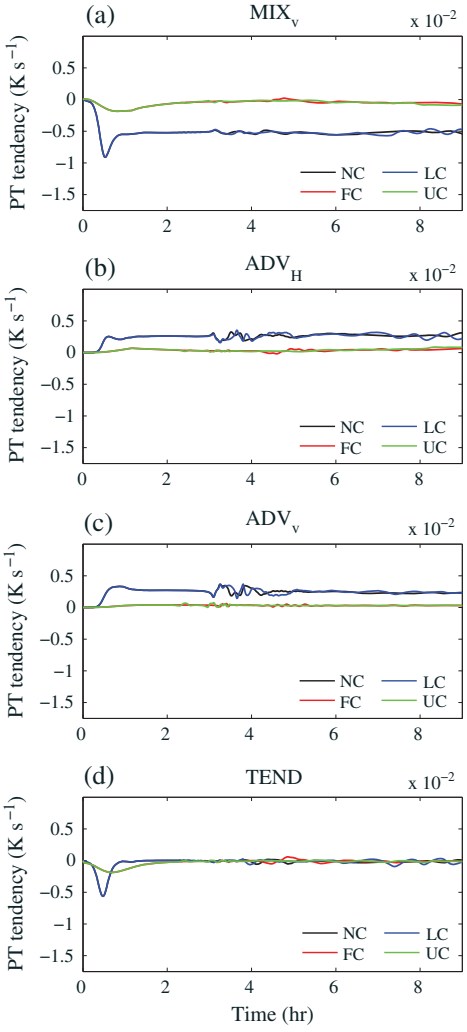

Figure 6. Time series of thermodynamic equation forcing terms, at point P_U. The terms are labeled as follows: MIX_V is vertical turbulent mixing, ADV_H and ADV_V are horizontal and vertical advection, and TEND is the sum of the four terms. Note that radiation flux divergence (RAD) and horizontal turbulent mixing (MIX_H) are omitted from the figure due to the small magnitude of those terms, compared to ADV and MIX_V. As in Figure 5, quantities are averaged from the surface to 18 m agl.

slope flow). First, consider the thermodynamic equation in the absence of precipitation processes,

$$\frac{\partial \theta'}{\partial t} = -w\frac{\partial \bar{\theta}}{\partial z} - \vec{u} \bullet \nabla\theta' + \bar{\rho}^{-1}\nabla \bullet \vec{H} + R \qquad (1)$$

In equation (1), θ refers to potential temperature, $\bar{()}$ and $()'$ refer to base state (function of height only) and perturbation variables, $\vec{u}$ is the total wind vector, and $\vec{H}$ is the three-dimensional turbulent heat flux. As in standard ARPS, heat flux is computed in ARPS-CANOPY as $\vec{H} = \bar{\rho}K_H(\nabla\theta)$, where $\bar{\rho}$ is base state density and K_H is the thermal turbulent diffusivity. From left to right in equation (1), the terms are time rate of change, or tendency, of perturbation potential temperature (TEND), adiabatic warming/cooling (ADAB), advection (ADV), turbulent mixing (MIX), and radiative forcing (RAD). Note that RAD is the sum of radiative forcing in the clearing fraction of each grid cell and the radiative forcing associated with radiative flux into or out of the canopy. For a full description of the ARPS governing equations, see *Xue et al.* [2000, 2001], and for details of the ARPS-CANOPY modifications, see *Kiefer et al*. [2013].

[23] Combining the first two terms on the right-hand side of equation (1) yields advection of total potential temperature and delineating between forcing in the horizontal and vertical dimensions (with respect to a Cartesian coordinate system) yields

$$\mathrm{TEND} = \mathrm{ADV}_H + \mathrm{ADV}_V + \mathrm{MIX}_H + \mathrm{MIX}_V + \mathrm{RAD} \qquad (2)$$

where subscripts H and V correspond to the horizontal and vertical components of forcing, respectively. In this and all subsequent budget analyses, the tendency term is calculated as a residual by summing each of the forcing terms on the right-hand side of equation (2). A comparison of the residual of equation (2) and the actual tendency computed from high-frequency model output (not shown) suggests that the residual provides a reasonable estimation of tendency.

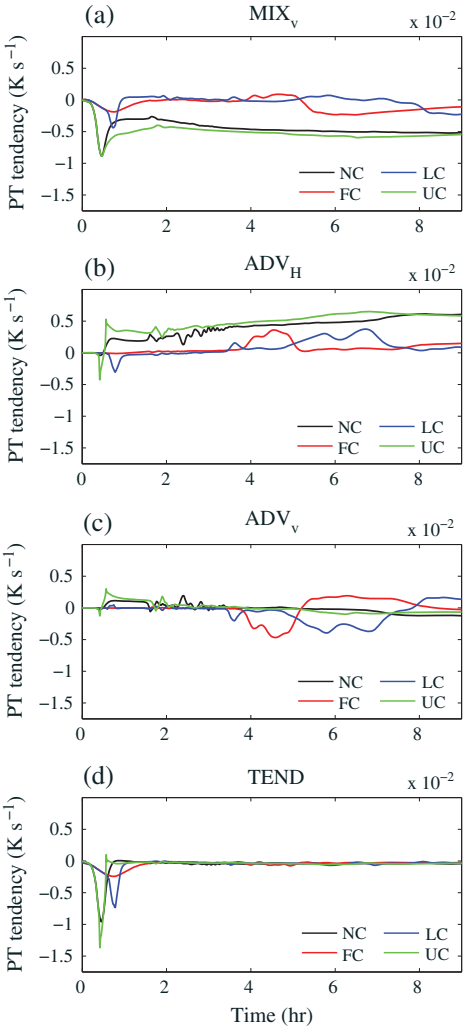

Figure 7. As in Figure 6 but at point P_L.

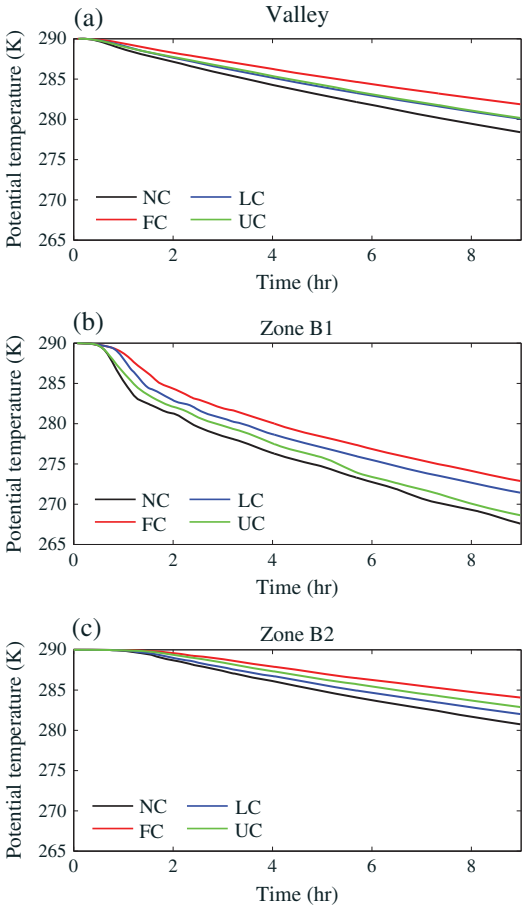

Figure 8. Time series of valley- and zone-average potential temperature. (a) Potential temperature averaged over the entire valley atmosphere; (b, c) potential temperature averaged across subdivisions of the valley atmosphere, denoted zone B1 (lower valley; $z < 170$ m msl) and zone B2 (upper valley; $170 < z < 500$ m msl).

[24] In Figures 6 and 7, time series of MIX_V, ADV_H, ADV_V, and TEND are presented, averaged from the surface to 18 m above ground level (AGL) at points P_U and P_L. Although RAD may be important near the surface in basins with very weak wind speeds [*Katurji and Zhong*, 2012] or in thick canopies [*Sun et al.*, 2006], when vertically averaged, the term is small compared to MIX_V and ADV in all four cases evaluated here. Thus, RAD (as well as MIX_H) is neglected in the following analyses. Examining the forcing terms at P_U first (Figure 6), we see that while MIX_V cools the near-surface atmosphere in all cases, the term is consistently largest in the cases with bare upper slopes (NC and LC) and smallest in the cases with forested upper slopes (FC and UC). For all terms, the magnitude and variation are determined by whether or not the site is covered by canopy. In other words, the two curves with canopy cover (FC and UC) collapse together while the two without canopy (NC and LC) merge together. Weaker cooling inside the canopy is expected since radiative cooling of the ground surface is weaker when trees are present. Furthermore, although canopy elements themselves cool rapidly as energy radiates upward from the canopy top, cooling of the adjacent air is considerably slower [*Froelich et al.*, 2011].

[25] Regarding advection, both ADV_H and ADV_V are of positive sign and largely offset the cooling from MIX_V in the cases with bare upper slopes, but are negligible in the cases with forested upper slopes (consistent with weak winds inside the canopy). As a result, the sum of all terms, TEND, exhibits a shorter duration, but stronger magnitude spike in cooling in the cases with bare upper slopes, and a longer duration, but weaker magnitude episode of cooling in the cases with forest cover on the upper slope. Thus, after about 2 h of simulation, the potential temperature difference between cases is small and the cooling trend is slow but steady (Figure 5a), as TEND in all cases is small and overall negative during the remainder of the simulation (Figure 6d).

[26] At the lower slope point, P_L, the thermodynamic budget interpretation is somewhat less straightforward,

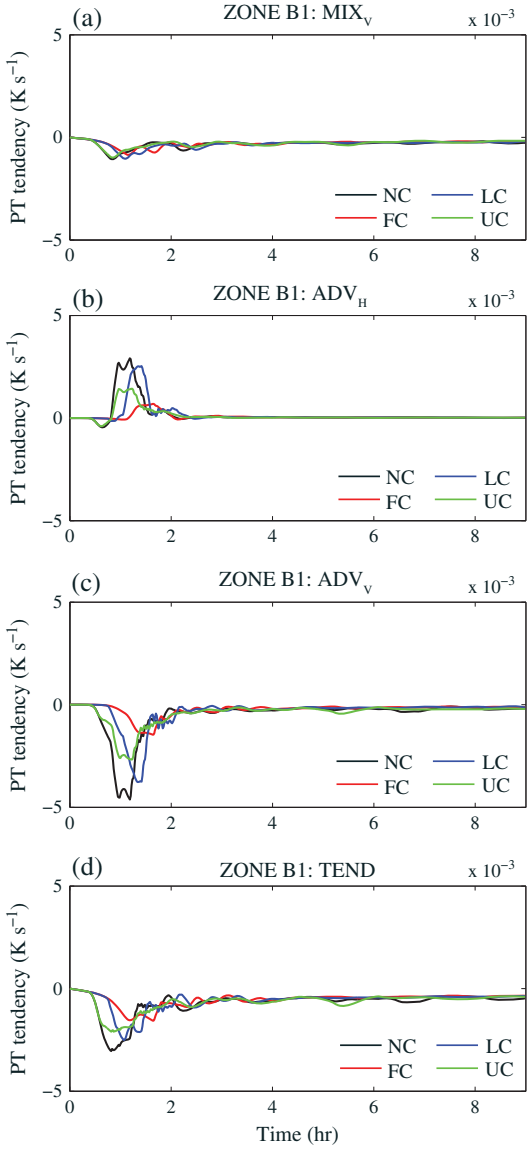

Figure 9. As in Figure 6 but averaged across all points in zone B1 (see Figure 1a for zone definition). Note change in y axis limits and scaling from Figure 6.

although the four terms also tend to form two groups depending on the presence or absence of a canopy at the site (Figure 7). MIX_V is consistently larger (i.e., more negative) in the cases with bare lower slopes (NC and UC), similar to the P_U analysis for bare upper slopes, and as was seen at the upper slope point, ADV largely offsets the cooling when trees are not present. The greatest difference in the thermodynamic budget between the upper and lower slopes is found in the LC case. About 45 min after initialization, a short duration peak in cooling due to MIX_V and ADV_H occurs. The sum of all terms (TEND) shows a spike in cooling weaker than in cases NC and UC but considerably stronger than in the case with full forest cover (FC). Referring back to the time series of maximum u component of wind at P_L (Figure 5d), we can attribute the spike in MIX_V and ADV_H to the intrusion of the well-developed downslope flow that developed over the bare upper slopes, on the forested lower slopes. However, from approximately T02 onward the total tendency is small and negative, consistent with the gradual cooling seen in Figure 5c.

[27] The episodes of enhanced MIX_V and ADV between T03 and T09 in the cases with lower slope forest cover (FC and LC) are the result of the downslope jet exit region gradually receding up the slope (Figures 2d and 2f) as the valley atmosphere cools, and air descending the slopes reaches its level of neutral buoyancy progressively farther up the slope as the night progresses [see *Whiteman et al.*, 2010; *Haiden et al.*, 2011]. During the later portion of the night, the jet exit region is in the vicinity of P_L in the FC and LC cases, where enhanced vertical transport of momentum and heat disturbs the otherwise quiescent atmosphere inside the forest. Regardless of the source of the enhanced MIX and ADV terms, the net tendency is small and close in magnitude to the cases with bare lower slopes (Figure 7d).

3.3. Valley Cooling Analysis

[28] With an understanding that the evolution of slope flow and the evolution of cooling in the valley atmosphere are intrinsically linked, we now consider the cooling of the valley atmosphere (and subdivisions of the valley) and investigate the role that forest cover along the valley sidewalls plays in that cooling. To achieve this goal, potential temperature is averaged over the entire valley atmosphere, and within two subdivisions of the valley atmosphere, zones B1 (lower valley; $z < 170$ m msl) and B2 (upper valley; $170 < z < 500$ m msl) (see Figure 1a). The reader is reminded that cooling rates simulated in this study may be exaggerated compared to valleys where cold air is able to drain downvalley.

[29] In Figure 8, time series of valley- and zone-average potential temperature reveal notable differences in cooling between individual cases and zones. In Figure 8a, we see that the difference in valley-mean potential temperature between cases NC and FC grows with time, eventually reaching about 4 K at T09, while valley-mean potential temperature is nearly identical in the LC and UC cases. Examining the mean potential temperature in zones B1 and B2, we see that the difference in zone-averaged potential temperature between cases NC and FC is about 6 K in zone B1 and 4 K in zone B2. In contrast to the valley-mean quantity, zone averaging reveals important differences between cases LC and UC. Differences between the partially forested cases are most pronounced in zone B1, although small, but persistent differences also exist in potential temperature averaged across zone B2. The maximum difference in mean potential temperature between cases LC and UC is about 3 K in zone B1 and 0.5 K in zone B2 (cf. Figures 8b and 8c). What is most critical here is the fact that zone B1 mean potential temperature is colder in case UC than in case LC, while in zone B2 the opposite is true. This is further evidence of the phenomenon seen earlier in the potential temperature profiles at points P_L and P_C (Figure 3); cooling in approximately the lower third (upper two thirds) of the valley atmosphere is most sensitive to forest cover along the lower half (upper half) of the mountain slope.

[30] Examining the thermodynamic forcing terms averaged across zone B1 (Figure 9), we see that ADV_V is the primary source of cooling, with MIX_V a secondary source. ADV_V cools as a result of upward motion (not shown),

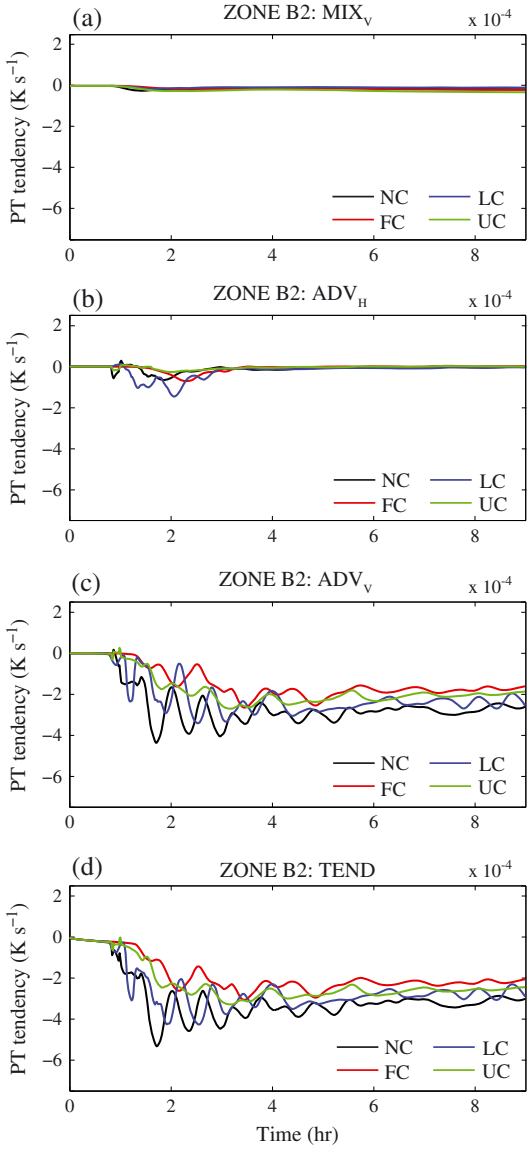

Figure 10. As in Figure 9 but averaged across all points in zone B2 (see Figure 1a for zone definition). Note change in y axis limits and scaling from Figure 9.

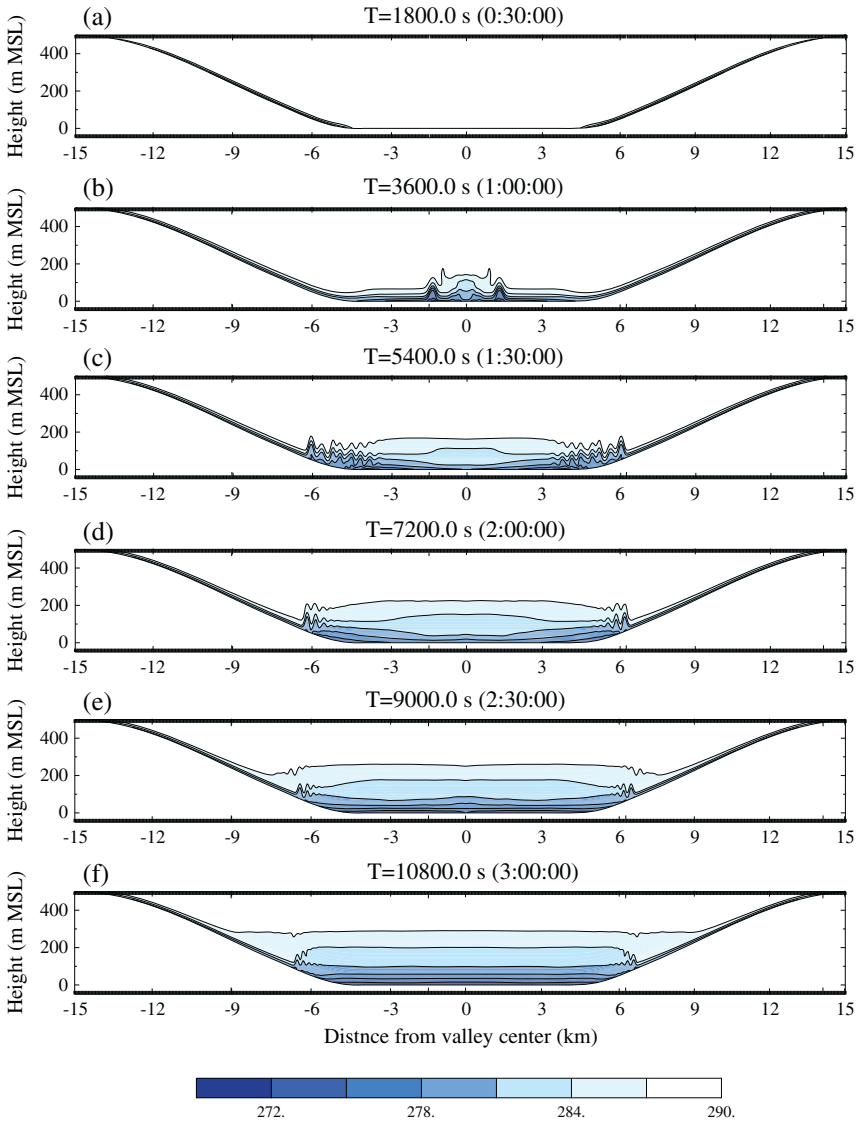

Figure 11. Vertical cross sections of potential temperature (K) for entire valley, from NC case, beginning 30 min after initialization and ending at T03. The time interval between panels is 30 min.

itself a by-product of the flux of mass into the valley (i.e., downslope flow) and mass conservation. The resultant adiabatic cooling has been shown in previous studies to be a primary source of cooling in basins and valleys, away from the ground surface [*Whiteman et al.*, 2010; *Kiefer and Zhong*, 2011; *Katurji and Zhong*, 2012]. Note that because the 2-D model configuration prohibits simulation of mass flux out of the valley, the upward motion (and cooling rates) simulated in this study may be somewhat exaggerated. In contrast to ADV_V, ADV_H warms the atmosphere, following a brief period of cooling associated with the arrival of the cold downslope flow in the center of the basin (see cooling in Figure 9b prior to T01). Evaluating the sum of all terms (TEND), we find that the cases with bare lower slopes (NC and UC) exhibit an earlier onset of cooling during the evening and also experience a longer duration of cooling, compared to the cases with forested lower slopes (FC and LC). Although the peak of TEND is larger in LC than UC, the cooling in LC is delayed compared to UC and is not as persistent (the net cooling is greater in UC).

[31] The thermodynamic budget in zone B2, farther away from the ground surface than zone B1, is dominated by ADV_V, with ADV_H a secondary source of cooling and MIX_V negligible (Figure 10). The most notable difference from the zone B1 budget assessment is the wavy appearance of ADV_V. Although waviness is somewhat apparent in zone B1 (Figure 9c), the scaling of the y axis largely masked the phenomenon there. The waviness is evidence of cold-air sloshing inside the valley during the developing stage of the cold-air pool. Potential temperature vertical cross sections during the first 3 h of the simulation (Figure 11) show the cold air pouring down the slopes, colliding in the center of the valley, and then sloshing back and forth thereafter, with the intensity of sloshing diminishing with time. The sign of ADV_V is consistently negative (i.e., cooling), but the wavy pattern results in large variations in magnitude with time. Despite the oscillations, it is clear that TEND is strongest

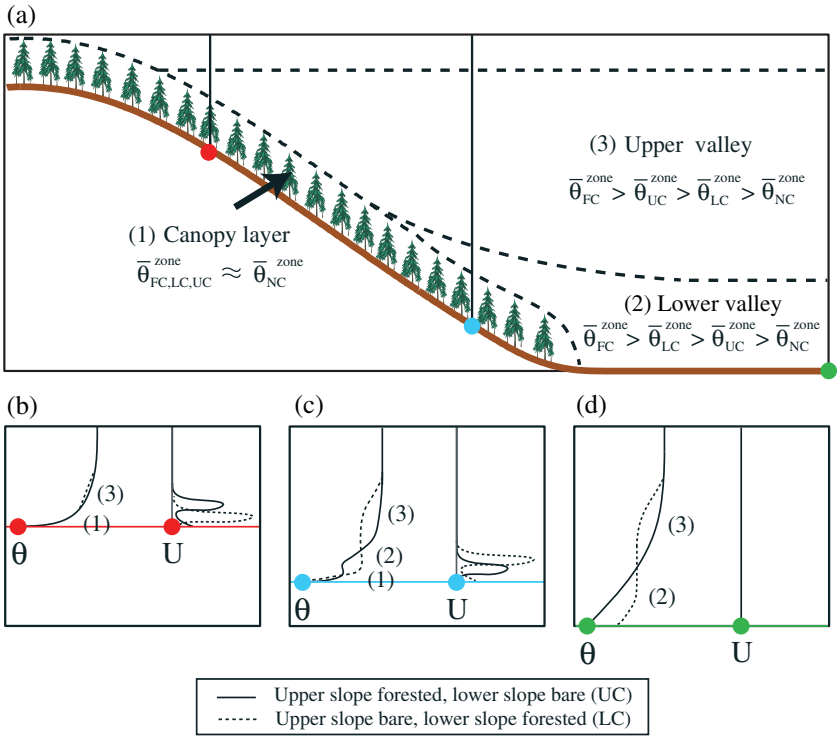

Figure 12. Conceptual model of downslope flow and cold-air pool characteristics in valleys with partially or fully forested sidewalls, approximately 6 h after local sunset; as in Figure 2, only the west half of the valley is depicted due to symmetry around the valley center. As seen in Figure 12a, a valley with total or partial tree cover may be divided into three layers: the canopy layer, and the upper and lower valley layers. Note that in Figure 12a, the canopy layer is exaggerated vertically for clarity. The symbol $\overline{\theta}^{zone}$ in Figure 12a refers to zone-averaged potential temperature. In Figures 12b–12d, profiles of θ and the u component of the wind (U) are displayed at points along the upper and lower slope, and at the valley center [location of points denoted by colored circles in Figure 12a]. In Figures 12b–12d, the solid line refers to the case with forested upper slopes and bare lower slopes (i.e. case UC) and the dashed line refers to the case with bare upper slopes and forested lower slopes (i.e., case LC). Labels to the right of the θ profiles correspond to the zones defined in Figure 12a.

in the cases with bare upper slopes (NC and LC), weakest in the cases with forested upper slopes (FC and UC), and is dominated by vertical advection in all cases. The larger magnitude of ADV_V in case LC (compared to UC) is consistent with the stronger slope flow at P_U (Figure 5b): Stronger mass flux into the valley implies stronger upward motion and adiabatic cooling.

4. Summary and Conclusions

[32] In this study, we have examined the impact of sidewall forest cover on diurnal cold-air pool evolution and the underlying dynamics. We utilized a recently developed canopy flow modeling system, ARPS-CANOPY, to perform numerical simulations with a two-dimensional domain. Four experiments were conducted with forest cover along the valley sidewalls varied from bare to partially forested to completely forested. The impact of forest cover on sidewall cooling and downslope flow was analyzed and related to the evolution of the cold-air pool inside the valley, while the evolution and dynamics of the cold-air pool were evaluated for the valley atmosphere as a whole and individual zones of the valley. A summary of the model results is presented in Figure 12.

[33] As shown in Figure 12a, the atmosphere in a valley with partially or fully forested sidewalls may be divided into three zones: the canopy layer, the lower valley, and the upper valley. Regardless of which portion of the valley atmosphere one considers, the coldest potential temperatures in the valley occur when the sidewalls are completely bare (NC), and the warmest potential temperatures occur when the sidewalls are completely forested (FC). Such differences were found to be associated with weaker surface cooling beneath the forest canopy (especially during the first 90 min of the simulation) and increased drag on air flowing down the sidewalls, when trees are present; the net result of the canopy processes is a weaker downslope flow. Thermodynamic budget analysis revealed that the weaker cooling rates in a valley with forested sidewalls occur primarily due to weaker vertical advection. Since upward motion is a consequence of mass continuity, retarded downslope flow (and mass flux into the valley) when the sidewalls are covered with trees leads to weaker upward motion and weaker adiabatic cooling. However, when averaged along the entire sidewall, potential temperature within the lowest 15–20 m above the ground is approximately equal between cases. Although near-surface cooling during approximately

the first 90 min after model initialization is stronger when the sidewalls are bare, the warming effect of advection (stronger in the cases with bare sidewalls) largely balances the cooling, resulting in similar canopy-layer-mean potential temperatures in the bare and forested cases during the remainder of the night. Although not shown, an additional experiment with forest cover along both the sidewalls and valley floor exhibited warmer near-floor potential temperatures, relative to the FC case, but potential temperatures and wind elsewhere in the valley were largely unaffected by the valley-floor forest cover.

[34] The limited number of research studies that have examined the impact of forest cover on nocturnal cooling inside valleys has generally identified forest cover as promoting cooling [e.g., *Gross*, 1987, *Gustavsson et al.*, 1998]. Our findings suggest that forest cover on sidewalls retards cooling inside valleys, mainly through weaker katabatic flows and subsequently, weaker adiabatic cooling. While we cite *Gross* [1987] in this study, we do so with caution, since the aforementioned limitations of their canopy parameterization and the combination of coarse grid spacing and complex valley topography render their results questionable. Furthermore, the importance of katabatic flows to valley atmosphere cooling distinguishes our study from *Gustavsson et al.* [1998], where shallow valleys with minimal katabatic flows were the primary focus. In their study, the role of the forest canopy was mainly as a wind shelter, allowing strong cooling to occur near the valley bottom in an otherwise mixed lower atmosphere. In our study, the principle effect of the forest canopy is to weaken katabatic flows in a valley where such flows are the principle driver of cold-air pools. Future numerical modeling studies may be useful in determining at what scale of valley the role of the forest canopy changes from primarily cooling to warming.

[35] Regarding the intermediate forest cover cases (LC and UC), potential temperature across the lower valley zone (roughly the lowest third of the valley atmosphere) is colder in the case with the lower half of the slopes bare and upper slopes forested (UC), while in the upper valley zone (roughly the upper two thirds of the valley atmosphere), potential temperatures are colder in the case with the upper half of the mountain slope bare and the lower slopes forested (LC). In a more general sense, we expect that nocturnal cooling in any given layer of a valley atmosphere will be most sensitive to sidewall forest cover at approximately the same height above the valley floor as that layer.

[36] Profiles of potential temperature and horizontal wind speed at points along the sidewall and in the valley center (Figures 12b–12d) depict a scenario in which differences in potential temperature between cases grow as one moves down the sidewall slope to the valley center, and in which downslope flow along the entire slope is largely determined by the state of forest cover on the upper slopes. Along the upper slopes (Figure 12b), potential temperature differs little between the intermediate cases (LC and UC), but pronounced differences in wind speed occur; the downslope jet is weaker and displaced away form the surface when trees are present. At the lower slope point (Figure 12c), potential temperature in the lower valley atmosphere is sensitive to forest cover along the lower slope, but the relationship of downslope jet speed to local forest cover is dominated by upstream effects. The strength of downslope flow is highly sensitive to the presence or absence of trees farther up the slope. At the valley center (Figure 12d), differences in potential temperature between cases peak, while quiescent conditions are present throughout the valley in each case.

[37] Before concluding, it is important to recall several limitations of this study. First and foremost, the findings are based on two-dimensional simulations. Limitations of a two-dimensional framework include the inability of a 2-D model to properly represent the downscale energy cascade, and the lack of complicating factors such as along-valley flow that cannot be simulated without the third dimension. In addition to the two-dimensional limitations, incomplete model radiation physics may affect the interpretation of our results. As the ARPS model only considers the vertical component of radiative fluxes, the effect of the horizontal component of radiative flux from the sidewalls on the temperatures inside the valley is not accounted for. Additionally, we do not consider the impact of urban canopies on cold-air pool evolution, an important detail that must be taken into account when considering valleys like the Salt Lake valley. Furthermore, canopy shape and density vary widely, and we have only considered one basic profile. Lastly, only quiescent conditions were considered in this study, eliminating any influence of dynamic pressure gradients along the slope of the mountain that can alter the flow up or down the forested slope [*Belcher et al.*, 2012].

[38] Notwithstanding such limitations, this study has provided valuable new insight regarding the sensitivity of slope flow and cold-air pool development to forest cover along valley sidewalls. Furthermore, this study has shown that ARPS-CANOPY can be a useful tool for addressing questions about cold-air pool processes in vegetated valleys, questions we have only begun to answer in this current study. Future efforts will address the sensitivity of cold-air pool evolution and dynamics to upstream conditions (e.g., wind speed, static stability), valley dimensions (e.g., width, depth), canopy characteristics (e.g., morphology, density), and forest patterns not evaluated in the current study (e.g., gradual along-slope vegetation changes). Although two-dimensional simulations are expected to remain the primary vehicle for this work, three-dimensional simulations must also be utilized in order to assess any impacts from the 2-D model limitations outlined earlier. In addition to the important findings of this study, such future work is expected to provide further insight into cold-air pool evolution and processes in forest-covered complex terrain.

[39] **Acknowledgments.** This research was supported by the U.S. National Science Foundation Physical and Dynamic Meteorology Division through grants AGS-0938401 (primary) and ATM-0837860 (secondary). Any opinions, findings, and conclusions or recommendations expressed are those of the authors and do not necessarily reflect the views of the National Science Foundation. We wish to thank three anonymous reviewers for their helpful comments and suggestions regarding the manuscript, and we also thank Marwan Katurji for useful discussions regarding the study and assistance with post-processing scripts. All simulations were performed on the NCAR supercomputer *Bluefire*, managed and operated by the Computational and Information Systems Laboratory (CISL).

References

Aubinet, M., B. Heinesch, and M. Yernaux (2003), Horizontal and vertical CO_2 advection in a sloping forest, *Boundary Layer Meteorol.*, *108*, 397–417.

Barr, S., and M. M. Orgill (1989), Influence of external meteorology on nocturnal valley drainage winds, *J. Appl. Meteorol.*, *28*, 497–517.

Belcher, S. E., I. N. Harman, and J. J. Finnigan (2012), The wind in the willows: Flows in forest canopies in complex terrain, *Annu. Rev. Fluid Mech.*, *44*, 479–504.

Chen, Y., F. L. Ludwig, and R. L. Street (2004), Stably stratified flows near a notched transverse ridge across the Salt Lake valley, *J. Appl. Meteorol.*, *43*, 1308–1328.

Chou, M.-D. (1990), Parameterization for the absorption of solar radiation by O_2 and CO_2 with application to climate studies, *J. Clim.*, *3*, 209–217.

Chou, M.-D. (1992), A solar radiation model for climate studies, *J. Atmos. Sci.*, *49*, 762–772.

Chou, M.-D., and M. J. Suarez (1994), An efficient thermal infrared radiation parameterization for use in general circulation models, *Tech. Rep. NASA Tech. Memo 104606*.

Clements, C. B., C. D. Whiteman, and J. D. Horel (2003), Cold-air-pool structure and evolution in a mountain basin: Peter Sinks, Utah, *J. Appl. Meteorol.*, *42*, 752–768.

Dupont, S., and Y. Brunet (2008), Influence of foliar density profile on canopy flow: A large-eddy simulation study, *Agric. For. Meteorol.*, *148*, 976–990.

Dupont, S., and Y. Brunet (2009), Coherent structures in canopy edge flow: A large-eddy simulation study, *J. Fluid Mech.*, *630*, 93–128.

Froelich, N. J., and H. P. Schmid (2006), Flow divergence and density flows above and below a deciduous forest. Part II. Below-canopy topographic flows, *Agric. For. Meteorol.*, *138*, 29–43.

Froelich, N. J., H. P. Schmid, C. S. B. Grimmond, H.-B. Su, and A. J. Oliphant (2005), Flow divergence and density flows above and below a deciduous forest. Part I. Non-zero mean vertical wind above canopy, *Agric. For. Meteorol.*, *133*, 140–152.

Froelich, N. J., C. S. B. Grimmond, and H. P. Schmid (2011), Nocturnal cooling below a forest canopy: Model and evaluation, *Agric. For. Meteorol.*, *151*, 957–968.

Geiger, R. (1965), *The Climate Near the Ground*, Harvard University Press, Cambridge, Massachusetts.

Goulden, M. L., J. W. Munger, S.-M. Fan, B. C. Daube, and S. C. Wofsy (1996), Measurements of carbon sequestration by long-term eddy covariance: Methods and a critical evaluation of accuracy, *Global. Change. Biol.*, *2*, 169–182.

Gross, G. (1987), Some effects of deforestation on nocturnal drainage flow and local climate—A numerical study, *Boundary Layer Meteorol.*, *38*, 315–337.

Gustavsson, T., M. Karlsson, J. Bogren, and S. Lindqvist (1998), Development of temperature patterns during clear nights, *J. Appl. Meteorol.*, *37*, 559–571.

Haiden, T., C. D. Whiteman, S. W. Hoch, and M. Lehner (2011), A mass-flux model of nocturnal cold air intrusions into a closed basin, *J. Appl. Meteorol. Clim.*, *50*, 933–943.

Kanda, M., and M. Hino (1994), Organized structures in developing turbulent flow within and above a plant canopy, using a large eddy simulation, *Boundary-Layer Meteorol.*, *68*, 237–257.

Katurji, M., and S. Zhong (2012), The influence of topography and ambient stability on the characteristics of cold-air pools: A numerical investigation, *J. Appl. Meteorol. Climatol.*, *51*, 1740–1749.

Kiefer, M. T., and S. Zhong (2011), An idealized modeling study of nocturnal cooling processes inside a small enclosed basin, *J. Geophys. Res.*, *116*, D20127, doi:10.1029/2011JD016119.

Kiefer, M. T., S. Zhong, W. E. Heilman, J. J. Charney, and X. Bian (2013), Evaluation of an ARPS-based canopy flow modeling system for use in future operational smoke prediction efforts, *J. Geophys. Res. Atmos.*, doi:10.1002/jgrd.50491, in press.

Lee, X. (1998), On micrometeorological observations of surface-air exchange over tall vegetation, *Agric. For. Meteorol.*, *91*, 39–49.

LeMone, M. A., K. Ikeda, R. L. Grossman, and M. W. Rottach (2003), Horizontal variability of 2-m temperature at night during CASES-97, *J. Atmos. Sci.*, *60*, 2431–2449.

Mahrt, L., D. Vickers, R. Nakamura, M. R. Soler, J. Sun, S. Burns, and D. H. Lenschow (2001), Shallow drainage flows, *Boundary Layer Meteorol.*, *101*, 243–260.

Michioka, T., and F. K. Chow (2008), High-resolution large-eddy simulations of scalar transport in atmospheric boundary layer flow over complex terrain, *J. Appl. Meteorol. Climatol.*, *47*, 3150–3169.

Parker, M. D., and R. H. Johnson (2004), Structures and dynamics of quasi-2D mesoscale convective systems, *J. Atmos. Sci.*, *61*, 545–567.

Reddy, P. J., D. E. Barbarick, and R. D. Osterburg (1995), Development of a statistical model for forecasting episodes of visibility degradation in the Denver metropolitan area, *J. Appl. Meteorol.*, *34*, 616–625.

Savage, L. C., S. Zhong, W. Yao, W. J. O. Brown, T. W. Horst, and C. D. Whiteman (2008), An observational and numerical study of a regional-scale downslope flow in northern Arizona, *J. Geophys. Res.*, *113*, D14114, doi:10.1029/2007JD009623.

Smith, C. M., and E. D. Skyllingstad (2005), Numerical simulation of katabatic flow with changing slope angle, *Mon. Weather Rev.*, *133*, 3065–3080.

Smith, R. B., et al. (1997), Local and remote effects of mountains on weather: Research needs and opportunities, *Bull. Am. Meteorol. Soc.*, *78*, 877–892.

Steinacker, R., C. D. Whiteman, M. Dorninger, E. Mursch-Radlgruber, K. Baumann, S. Eisenbach, A. M. Holzer, and B. Pospichal (2007), A sinkhole field experiment in the Eastern Alps, *Bull. Am. Meteorol. Soc.*, *88*, 701–716.

Sun, H., T. L. Clark, R. B. Stull, and T. A. Black (2006), Two-dimensional simulation of airflow and carbon dioxide transport over a forested mountain. Part I: Interactions between thermally-forced circulations, *Agric. For. Meteorol.*, *140*, 338–351.

Thompson, B. W. (1986), Small-scale katabatics and cold hollows, *Weather*, *41*, 146–153.

Trachte, K., T. Nauss, and J. Bendix (2010), The impact of different terrain configurations on the formation and dynamics of katabatic flows: Idealized case studies, *Boundary Layer Meteorol.*, *134*, 307–325.

Whiteman, C. D., and S. Zhong (2008), Downslope flows on a low-angle slope and their interactions with valley inversions. Part I: Observations, *J. Appl. Meteorol. Climatol.*, *47*, 2023–2038.

Whiteman, C. D., T. B. McKee, and J. C. Doran (1996), Boundary layer evolution within a canyonland basin. Part I: Mass, heat and moisture budgets from observations, *J. Appl. Meteorol.*, *35*, 2145–2161.

Whiteman, C. D., S. Zhong, W. J. Shaw, J. M. Hubbe, X. Bian, and J. Mittelstadt (2001), Cold pools in the Columbia Basin, *Weather Forecasting*, *16*, 432–447.

Whiteman, C. D., et al. (2008), METCRAX 2006—Meteorological experiments in Arizona's Meteor Crater, *Bull. Am. Meteorol. Soc.*, *89*, 1665–1680.

Whiteman, C. D., S. W. Hoch, M. Lehner, and T. Haiden (2010), Nocturnal cold air intrusions into a closed basin: Observational evidence and conceptual model, *J. Appl. Meteorol. Climatol.*, *49*, 1894–1905.

Xue, M., K. K. Droegemeier, and V. Wong (2000), The Advanced Regional Prediction System (ARPS)—A multi-scale nonhydrostatic atmosphere simulation and prediction model. Part I: Model dynamics and verification, *Meteorol. Atmos. Phys.*, *75*, 463–485.

Xue, M., K. K. Droegemeier, V. Wong, A. Shapiro, K. Brewster, F. Carr, D. Weber, Y. Liu, and D. Wang (2001), The Advanced Regional Prediction System (ARPS)—A multi-scale nonhydrostatic atmosphere simulation and prediction tool. Part II: Model physics and applications, *Meteorol. Atmos. Phys.*, *76*, 143–165.

Xue, M., D. Wang, J. Gao, K. Brewster, and K. K. Droegemeier (2003), The Advanced Regional Prediction System (ARPS), storm-scale numerical weather prediction and data assimilation, *Meteorol. Atmos. Phys.*, *82*, 139–170.

Zhong, S., and C. D. Whiteman (2008), Downslope flows in a low-angle slope and their interactions with valley inversions. Part II: Numerical modeling, *J. Appl. Meteorol. Clim.*, *47*, 2039–2057.